Emergence of spatiotemporal dislocation chains in drifting patterns

M. G. Clerc, C. Falcón, M. A. García-Ñustes, V. Odent, and I. Ortega

Citation: Chaos: An Interdisciplinary Journal of Nonlinear Science **24**, 023133 (2014); doi: 10.1063/1.4883650
View online: http://dx.doi.org/10.1063/1.4883650
View Table of Contents: http://scitation.aip.org/content/aip/journal/chaos/24/2?ver=pdfcov
Published by the AIP Publishing

Emergence of spatiotemporal dislocation chains in drifting patterns

M. G. Clerc,[1,a)] C. Falcón,[1,b)] M. A. García-Ñustes,[2,c)] V. Odent,[1,d)] and I. Ortega[1,3]
[1]*Departamento de Física, Facultad de Ciencias Físicas y Matemáticas, Universidad de Chile, Casilla, 487-3 Santiago, Chile*
[2]*Instituto de Fisica, Pontificia Universidad Catlica de Valparaso Avenida Brasil, 2950 Valparaso, Chile*
[3]*School of Mathematics and Statistics, University of New South Wales, Sydney, New South Wales 2052, Australia*

(Received 30 December 2013; accepted 4 June 2014; published online 16 June 2014)

One-dimensional patterns subjected to counter-propagative flows or speed jumps exhibit a rich and complex spatiotemporal dynamics, which is characterized by the perpetual emergence of spatiotemporal dislocation chains. Using a universal amplitude equation of drifting patterns, we show that this behavior is a result of a combination of a phase instability and an advection process caused by an inhomogeneous drift force. The emergence of spatiotemporal dislocation chains is verified in numerical simulations on an optical feedback system with a non-uniform intensity pump. Experimentally this phenomenon is also observed in a tilted quasi-one-dimensional fluidized shallow granular bed mechanically driven by a harmonic vertical vibration. © *2014 AIP Publishing LLC*. [http://dx.doi.org/10.1063/1.4883650]

Nature is ripe with patterns and structures of different shapes and sized. These patterns naturally show imperfections where the pattern amplitude goes to zero, termed *defects*, which can display a rich and complex spatiotemporal dynamics. In this article, we show that when one-dimensional patterns are subjected to flows that change spatially their intensity, single defects or arrays of them appear constantly over the observed pattern in space and time. These defects are thus known as dislocations on the space-time evolution of the pattern, as they are similar the classical dislocations observed in solids or in the stripe patterns of bi-dimensional systems out of equilibrium. We explain this phenomenon theoretically using a universal model that describes how the amplitude of the moving pattern creates such defects through a combination of an phase instability of the pattern interacting with the inhomogeneous flow. The explanation of the continuous generation of defects in drifting patterns is verified by simulating numerically the proposed model. This verification is also performed on a more complex model describing the evolution of an optical feedback system with a non-uniform intensity pump. Furthermore, we observe experimentally the generation of spatiotemporal dislocation chains on a quasi-one-dimensional fluidized shallow granular bed mechanically driven by a harmonic vertical vibration, where the inhomogeneous flow is included by tilting the cell. In that sense, the results presented in this work are meaningful to the whole community involved in understanding the way defects interact within pattern forming systems and how their dynamics influence the long-term evolution of the underlying pattern.

I. INTRODUCTION

Non-equilibrium processes often lead to the formation of spatially periodic structures arising from an homogeneous state through the spontaneous breaking of symmetries present in the system under study.[1–5] Pattern formation is generally observed by modifying a single parameter, usually called bifurcation parameter, which controls the transition from an homogeneous state to a patterned one as it surpasses a certain threshold. In one-dimensional extended systems, when one continues increasing this parameter above threshold, the pattern can exhibit secondary instabilities, for example, spatial and temporal period doubling, oscillatory, Eckhaus, and parity breaking ones.[6] Secondary instabilities are generically the cause of the transition from motionless to propagative patterns. These transitions in pattern forming systems have been studied in several physical contexts, such as parametrically amplified surface waves in Newtonian[7] and non-Newtonian fluids,[8] fluidized granular beds,[9] binary fluid convection,[10] and nonlinear optics,[11] to mention a few. This phenomenon can be produced by two mechanisms: (i) spontaneous symmetry-breaking transitions, where the pattern will choose spontaneously the direction of its propagation depending on initial conditions,[2,12] and (ii) induced parity-breaking transitions, where stationary-to-propagating pattern bifurcations arise when motionless patterns are exposed to drift forces or spatial inhomogeneities.[9,11] In the latter case, patterns are commonly deformed and advected, which is usually related to the development of convective instabilities.[2]

The entire class of scenarios that can trigger the spatiotemporal evolution of drifting patterns have not been identified yet. Particularly, one expects a rich and complex spatiotemporal dynamics. Experimental observations of drifting patterns have been reported in particle-laden flows inside a partially fluid filled, horizontal, rotating cylinder,[13] a free electron laser[14] and a one-dimensional transverse Kerr-type slice subjected to optical feedback.[15] In the former work, the

[a)]Electronic mail: marcel@dfi.uchile.cl
[b)]Electronic mail: cfalcon@ing.uchile.cl
[c)]Electronic mail: mgarcianustes@ing.uchile.cl
[d)]Electronic mail: vodent@ing.uchile.cl

proposed physical mechanism for this phenomenon is based on nonuniformities of the control parameter, which induce an Eckhaus instability.[15,16] The aim of this letter is to study and explain the appearance of spatiotemporal dislocation chains in drifting patterns. Despite of experimental reports, the recognition of the nature and origin of this universal phenomenon and the ingredients necessary for its existence are absent. A dislocation chain is a defect line composed by phase singularities. The distance between neighboring singularities is of the same order of the underlying wavelength. Indeed, this spatiotemporal dynamics can be understood as a consequence of counter-propagative flows, speed jumps, or inhomogeneities in the parameters of drifting pattern systems. That is, the inhomogeneous spatial coupling is responsible of this phenomenon. Based on an amplitude equation describing the evolution of a pattern, we identify the mechanism for the emergence of spatiotemporal dislocation chains in the presence of a drift. This dynamical behavior is a combination of a phase instability–local Eckhaus instability–and an advection process caused by the inhomogeneous drift force. The appearance and dynamics of dislocation chains are numerically verified on a one-dimensional amplitude equation where the ingredients described above are present, and also on a model describing a transverse Kerr-type slice under to optical feedback illuminated by a non-uniform beam. Furthermore, the phenomenon is observed experimentally in a tilted quasi-one-dimensional fluidized shallow granular bed mechanically driven by harmonic vertical vibrations.

II. THEORETICAL DESCRIPTION OF DISLOCATION CHAINS

Let us consider a one-dimensional extended system described by the dimensionless partial differential equation

$$\partial_t \vec{u}(x,t) = \vec{f}(\vec{u}(x,t), \partial_x, \{\varepsilon\}) - v(x)\partial_x \vec{u}, \qquad (1)$$

where $\vec{u}(x,t)$ is a vectorial field that describes the system under study, $\{x,t\}$ respectively stand for the spatial and temporal coordinates, $\vec{f}$ is the vector field, $\{\varepsilon\}$ is a set of parameters that characterizes the system under study, and $v(x)$ accounts for an inhomogeneous drift force.

In the case of zero-drift, i.e., $v(x)=0$, we assume that the system possesses a stationary state $\vec{u}_0$ that satisfies $\vec{f}(\vec{u}(x,t), \partial_x, \{\varepsilon\}) = 0$, which exhibits a supercritical spatial instability at a critical wavenumber $k=k_c$ when one of the parameters surpasses a certain threshold, say ε_c, generating a stationary pattern.

Under suitable boundary conditions, when the pattern is subjected to a small constant drift force $[v(x) = v_o \neq 0]$, it remains motionless in a parameter region, i.e., there is a pinning range.[11] Above a critical value of the drift force, the pattern becomes propagative, which correspond to a regime of absolute instability.[2] Increasing further v_o, the system enters a convective instability regime where the drift is large enough to advect the patterned state away completely from the region under study, returning the system to an homogeneous state.[17]

The former scenario changes dramatically when we consider non-uniformities in the drift force $[v(x)]$. Physical

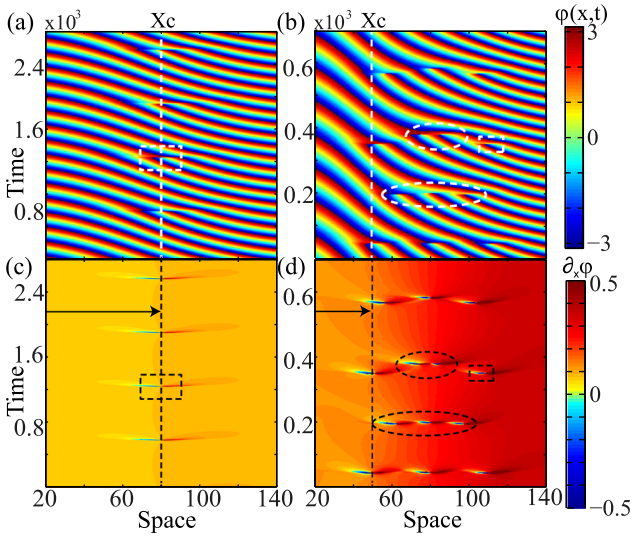

FIG. 1. Spatiotemporal dislocation chains in drifting patterns. (a) and (b) are spatiotemporal diagrams of the phase $\varphi(x,t)$ and (c) and (d) their respective phase gradients $\partial_x\varphi$ given by model Eq. (3). Simulation parameters are $\mu=0.4$, $dx=0.4$, $L=400$, $X_0=0$ with $\kappa=10^{-4}$ (left panel) and $\kappa=3\times10^{-4}$ (right panel), respectively. Dislocation chains and isolated defects are framed by dashed circles and squares, respectively. X_c corresponds to critical position.

transport processes such as inhomogeneous diffusion or dispersion and inhomogeneous spatial coupling can lead to an inhomogeneous drift force in the system. In such cases, the drifting pattern can be deformed creating regularly isolated or sequence of dislocations in the spatiotemporal diagram, which corresponds to singularities in the phase or hole solutions in the pattern envelope (see Figs. 1 and 2).

Examples of non-uniform drift forces can be encountered in different fields ranging from biology to chemistry to physics. For instance in physics, particle segregation in a

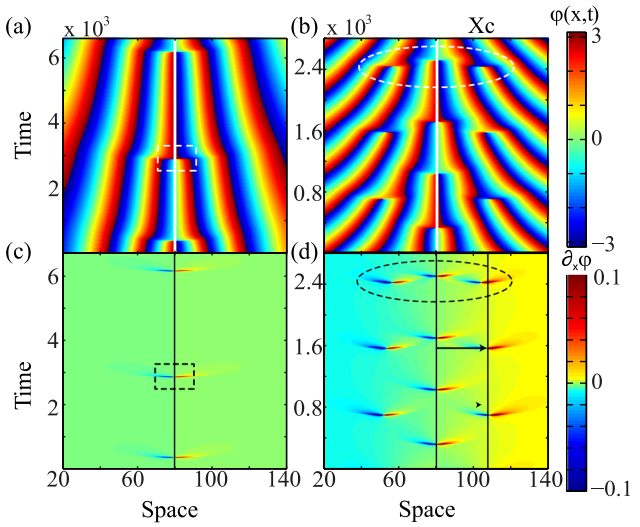

FIG. 2. Spatiotemporal dislocation chains in drifting patterns. (a) and (b) are spatiotemporal diagrams of the phase $\varphi(x,t)$ and (c) and (d) their respective phase gradients $\partial_x\varphi$ given by model Eq. (3). Simulation parameters are $\mu=0.4$, $dx=0.4$, $L=400$, $X_0=80$ with $\kappa=10^{-4}$ (left panel) and $\kappa=3\times10^{-4}$ (right panel), respectively. Dislocation chains and isolated defects are framed by dashed circles and squares, respectively. X_c corresponds to critical position.

laden flow inside a horizontal, rotating cylinder exhibit banding pattern formation.[13] The spatiotemporal dynamics shows two counter propagative drifts. Due to this non-uniform drift caused by the cylinder curvature, the pattern exhibits a continuous formation of defects. Another example is a liquid crystal layer subject to an inhomogeneous optical pump.[15] In this case, a Kerr medium slice is shined by a Gaussian laser beam which through optical feedback generates an inhomogeneous flow, locally advecting the pattern, creating dislocations in the spatiotemporal diagram.

A. Unified description

To understand in a unified manner the previously discussed phenomenon, we study the amplitude evolution at the onset of the spatial bifurcation assuming that the drift force varies smoothly compared with the pattern wavelength. Introducing the following *ansatz* for the critical propagative mode:

$$\vec{u}(x,t) = \mu^{1/2} A(X,T) e^{i(k_c x - v_0 t)} \vec{u}_k + c.c. + h.o.t., \qquad (2)$$

where $A(X,T)$ is the envelope of the propagative pattern, which is a slowly varying in time and space which scale as $X \equiv \mu^{1/2} x$, $T \equiv \mu t$, respectively, *c.c.* and *h.o.t.* stand for complex conjugate and higher order terms, see Ref. 2. $\vec{u}_k$ is the marginal mode at ε_c with wavenumber k_c. The corresponding amplitude equation close to threshold is the Ginzburg-Landau equation

$$\partial_T A = \mu_0 A - |A|^2 A + \partial_{XX} A - i\tilde{v}(X) A, \qquad (3)$$

where $\mu_0 \equiv (\varepsilon - \varepsilon_c)/\mu$ and $\tilde{v}(X) \equiv [v(X) - v_0]k_c/\mu$ is a spatial function accounting for the effect of the inhomogeneous drift force. Using polar fields representation of the amplitude, $A = Re^{i\varphi}$, one introduces two scalar fields $R(X,T)$ and $\varphi(X,T)$, the magnitude and phase of the amplitude, respectively.

B. Derivation of the amplitude equation in a simple model

In order to illustrate the above procedure, let us consider the following prototype model of pattern formation with drifting force (supercritical drifting Swift-Hohenberg):

$$\partial_t u = \mu u - u^3 - \left(\partial_{xx} + q^2\right)^2 u - \gamma(x)\partial_x u, \qquad (4)$$

where $u(x,t)$ is a scalar field, μ is the bifurcation parameter, q is the pattern wavenumber, and γ accounts for drift source of the pattern. The Swift-Hohenberg model was introduced to describe the onset of Rayleigh-Benard convection; however, recent generalizations have been used intensively to account for pattern formation in several systems.[2] Equation (4) under the influence of a small drifting force ($\gamma(x) \ll 1$) describes a spatial supercritical bifurcation. For $\mu < 0$, the system presents a stable uniform state $u(x,t) = 0$. At $\mu = 0$, the system bifurcates, the uniform solution becomes unstable, giving rise to pattern formation. For $\mu > 0$, the pattern amplitude, at wavenumber $k_c = \pm q$, grows as the square root of μ.

To describe the dynamics of the pattern at the onset of bifurcation ($\mu \ll 1$), we introduce the *ansatz*

$$u(x,t) = \frac{A(T,X)}{\sqrt{3}} e^{iqx} + \frac{\bar{A}(T,X)}{\sqrt{3}} e^{-iqx} + W(A,\bar{A},x), \qquad (5)$$

where A accounts for the amplitude of the critical mode q, which varies slowly in space and time ($\partial_{XX} A \ll \partial_X A \ll 1$ and $\partial_T A \ll 1$) and $W(A,\bar{A},x)$ is a small correction function including high order terms in A and $\bar{A}$. Introducing the above *ansatz* in Eq. (4), linearizing in W and considering the dominant terms, we get

$$\left(\partial_{XX} + q^2\right)^2 W = \frac{A^3}{3\sqrt{3}} e^{i3qx} + \left\{ -\partial_T A + \mu A - |A|^2 A + 4q^2 \partial_{XX} A - iq\gamma A \right\} \frac{e^{iqx}}{\sqrt{3}} + c.c.$$

To solve the above equation, we must to impose the following solvability conditions:[3]

$$\partial_T A = \mu A - |A|^2 A + 4q^2 \partial_{XX} A - iq\gamma(X) A, \qquad (6)$$

and then

$$W(A,\bar{A},x) = \frac{A^3}{2^6 3^{3/2}} e^{i3qx} + \frac{\bar{A}^3}{2^6 3^{3/2}} e^{-i3qx}. \qquad (7)$$

Then, one simultaneously determines the change of variable [Eq. (5)] and the amplitude equation of the critical mode [Eq. (6)]. Note that the Eq. (6) is valid considering the following scaling $A \sim \mu^{1/2}$, $\partial_T \sim \mu$, $\partial_X \sim \mu^{1/2}$ and $\gamma \sim \mu$. Normalizing the spatial scale and the coefficients in Eq. (6), one obtains the amplitude Eq. (3).

C. Mechanism of spatiotemporal dislocations chain

Numerical simulations of amplitude Eq. (3) show the formation of spatiotemporal dislocation chains (see Fig. 1). We consider Eq. (3) with Neumann boundary conditions, i.e., $\partial_X A(0,t) = \partial_X A(L,t) = 0$, for any t, where L is the system size. Equation (3) is simulated with a 4th order Runge-Kutta solver where the temporal step $dt = 0.02$ and with a finite difference solver with a spatial step $dx = 0.4$.

For the sake of simplicity, we consider a linear ramp forcing of the form $v(X) = \kappa(X - X_0)$ ($\kappa \ll 1$), where X_0 is the point when $\tilde{v}(X) = v_0 k_c/\mu$. The phase $\varphi(X,T)$ (Figs. 1(a) and 1(b)) and the phase derivative $\partial_x \varphi(X,T)$ (Figs. 1(c) and 1(d)) are shown for different values of κ with $X_0 = 0$. In this case, only a left pointing drift appears. Successive appearances of phase instabilities are observed. For small values of κ, we observe the appearance of isolated dislocations at a distance X_c from $X_0 = 0$. For larger values of κ, formation of dislocation chains is observed.

For a uniform drift ($\kappa = 0$), the amplitude Eq. (3) has a family of periodic solution $A_p(X) = \sqrt{\mu_0 - p^2} e^{ip(X - X_0)}$, parametrized by a continuous parameter $p < \sqrt{\mu_0}$. This family describes an homogenous pattern, which goes through a

phase instability at $p = p_c$, where $p_c^2 \equiv \mu_0/3$, corresponding to the well-known Eckhaus instability threshold.[2] To describe the dynamics in the inhomogeneous media, Eq. (3), we promote the parameter p to a function of space, which at dominant order is quadratic function of X. Thus, we propose the *ansatz*

$$A_p(Z = X - X_0) \approx \sqrt{\mu_0 - \left(p + \frac{\kappa}{6}Z^2\right)^2}\, e^{i\left(p+\frac{\kappa}{6}Z^2\right)Z}, \quad (8)$$

which corresponds to a pattern with increasing modulus and phase as a function of the spatial coordinate. The Eckhaus instability is characterized by the local deformation of phase gradients, which generates phase singularities and, respectively, hole solutions on the envelope modulus. Later, the pattern modifies locally its wavenumber, diffusing it within itself and finally materializing a stable pattern state. From expression (8), using the Eckhaus instability criterium, the inhomogeneous pattern state becomes unstable at a critical position

$$X_c(p) = sgn(\kappa)\sqrt{\frac{6}{|\kappa|}}\left[\sqrt{\frac{\mu_0}{3}} - |p|\right]^{1/2}. \quad (9)$$

Notice that the critical distance is a function of the wavenumber of the pattern that is parametrized by p. Therefore, these phase singularities generated at this position are advected as a consequence of the drift force, restarting the process. Hence, the system exhibits the perpetual creation of spatiotemporal dislocations as a result of the above process. As in the case of the Eckhaus instability, depending on initial conditions, it is possible to generate several phase singularities on different locations of the pattern, which diffuse the stable wavelength. Then, when κ^{-1} is larger than the size of phase singularities ($\kappa > \sqrt{\mu}$), the system presents the formation of dislocation chains. If we consider counter propagative flows at a confluence point X_0 ($X_0 \neq 0$), a similar behavior composed by two opposite propagative patterns is observed in the region of confluence (cf. Fig. 2). For $\kappa > 0$ ($\kappa < 0$), the defects annihilate (create) successively. For small κ, we observe the annihilation (creation) of defects only in the confluence region. For greater values of κ, the pattern starts to destabilize at a distance X_c from X_0, creating new defects at each side. We like to emphasize that the former dynamical behavior was equally observed in our numerical simulations with periodical boundary conditions.

III. OPTICAL SPATIOTEMPORAL DISLOCATION CHAINS

As an example of the former dynamics in a physical system, we have conducted numerical simulations of a one-dimensional transverse Kerr-type slice with optical feedback shined by a non-uniform laser beam.[15] This system is composed of a nematic liquid crystal sample (Kerr media represented in Fig. 3(a) by LC) and a mirror, which is illuminated with a non-uniform beam, which crosses first the liquid crystal layer, then reflected on the mirror and re-crosses the liquid crystal layer. Figure 3(a) depicts a schematic sketch of the transverse Kerr-type slice with optical feedback. The numerically simulated nonlinear medium is assumed to be a 50 μm thick layer of E7 nematic liquid crystal with homeotropically anchored. The laser beam is chosen as monomode frequency source, $\lambda_0 = 532$ nm and unidimensional (1D) following the x axis (see Fig. 3(a)), which can be produced by cylindrical lenses for instance. The laser field profile is represented by a stationary linear ramp function, as $F(x) = F_0(1 - x/2L)$, where $|F_0|^2$ is the maximum laser intensity and $L = 1.6$ mm is the system size. This kind of profile is feasible experimentally with a Spatial Light Modulator. $B(x,t)$ is the backward field which crosses the slide, which is reflected by the mirror M. This field is directly reinjected itself onto the slide from the back. Notice that this field is depend on space and time because its phase is modified by the liquid crystal refractive index when it crosses the sample. R is the mirror intensity reflectivity, which is positioned at a distance d of the liquid crystal sample. The modification of the refractive index $\delta n(x,t)$ induced by light with respect to the unperturbed refractive index n_0 is a satisfactory order parameter to describe the dynamics of this system. Thus, we will concern ourselves with $n(x,t) = n_0 + \delta n(x,t)$, where $n(x,t)$ is the effective refractive index of the Kerr-type slice and $\delta n \ll n_0$. Hence, $\delta n(x,t)$ satisfies[18,19]

$$\tau\frac{\partial \delta n}{\partial t} = -\delta n + l_d^2\frac{\partial^2 \delta n}{\partial x^2} + |F(x)|^2 + |B(x,t)|^2, \quad (10)$$

with τ is the relaxation time of the liquid crystal molecules, and l_d is the diffusion length. The explicit form of $B(x,t)$ is given by[18,19]

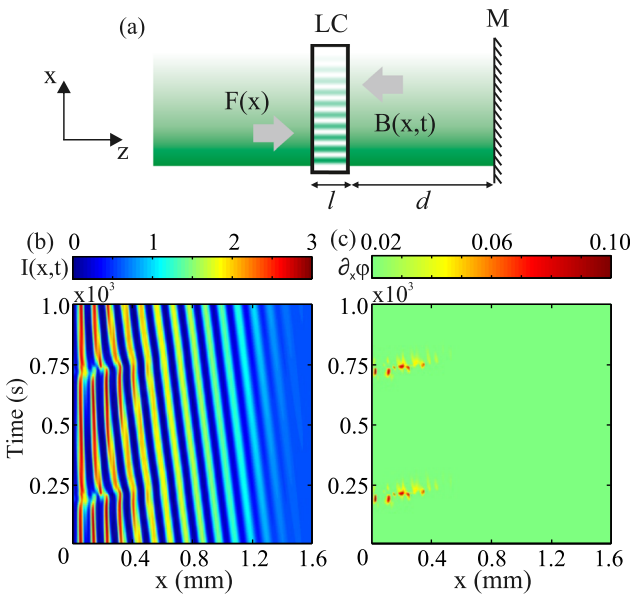

FIG. 3. Spatiotemporal dislocation chains in 1D optical Feedback with linear transverse pumping. (a) Schematic sketch of the Kerr-type slice with optical feedback. M is the mirror, LC is the liquid crystal, and F and B are the forward and the backward fields. (b) Drifting pattern with long dislocation chains. (c) Local phase gradient. $F_0 = 1.1$, $d = 5$ mm, $\lambda_0 = 532$ nm, $\chi l = 1$, $l_d = 10\,\mu$m, and $\tau = 2.23$ s. $F(x) = F_0\left(1 - \frac{x}{2L}\right)$, with $L = 512$. $I(x,t) = |B(x,t)|^2$.

$$B(x,t) = \sqrt{R}e^{\frac{id\lambda_0}{2\pi}\partial_{xx}}(e^{i\chi l\delta n(x,t)}F(x)),$$

where λ_0 is the laser wavelength, χ is the coefficient of the Kerr nonlinearity, and l is the liquid crystal sample thickness. We assume that free space propagation length is much bigger that the liquid crystal sample thickness, $d \gg l$, to neglect the diffraction in the nonlinear medium. When F_0 exceeds a critical value $F_{0c} \equiv (k_c^2+1)/2R\chi\sin(k_c^2 d\lambda_0/2\pi)$, the refractive index exhibits a spatial modulation instability with wavenumber $k_c = \pi/(d\lambda_0)$.[19] Based on the amplitude equation method, close to the spatial instability, we can introduce the *ansatz* $n(x,t) = Ae^{ik_c x}/\sqrt{\rho} + h.o.t$, where $\rho = RF_{0,c}\chi^2[3\chi\sin(\sigma k_c^2) - \chi\sin(3\sigma k_c^2) + 2a_1\chi(\cos(\sigma k_c^2) - \cos(3\sigma k_c^2))]$ in Eq. (10), and we get at dominant order the amplitude Eq. (3) with

$$\mu_0 = \frac{2R(F_0 - F_{0,c})\chi\sin(\sigma k_c^2)}{F_{0,c}}, \qquad \tilde{v}(x) = \frac{2RF_{0,c}\chi k_c\sin(\sigma k_c^2)}{2L}x. \tag{11}$$

Therefore, we expect that this system exhibits spatiotemporal dislocation chains. To verify the above predictions, we conducted numerical simulations of model (10) with a variable step of RungeKutta order 8 solver (dop853)[20] and with periodical boundary conditions. We perform the spatial derivatives using the Fourier space (FFTW3 Library) with a spatial step $dx = 0.27\ l_d$. Figure 3 displays a numerical simulation of Eq. (10) considering the linear forward propagation profile $F(x)$. Such profile generates a non-uniform drift in one direction, as we can see in Fig. 3(b) where the intensity has been displayed as a function of time. Close to the left border, the formation of sequences of dislocation chains can be observed. As seen in Fig. 3(c), these sequences correspond to phase singularities. Thus, the optical feedback system verifies the appearance of spatiotemporal dislocation chains when this is subjected to an inhomogeneous drifting force as predicted by amplitude Eq. (3).

IV. GRANULAR DISLOCATION CHAINS

The phenomenon theoretically explained above was also observed experimentally on a simple fluidized granular system, which presents drifting patterns. The experimental setup is depicted in Fig. 4(a). A container ($60 \times 40 \times 7\ \text{mm}^3$) made out of two 5 mm thick plexiglas walls with a aluminum frame between them holds in the space between the walls 4.0 g of monodisperse brass spheres of diameter $D = 150\ \mu$m, creating a granular layer 1.7 mm in depth. In units of grain diameters, the granular layer is approximately 400 D wide, 47 D in thickness, and 12 D in depth. The cell is mounted on an electromagnetic vibration exciter, driven by a frequency synthesizer (FS), via a power amplifier (Amp), providing a vertical sinusoidal acceleration (horizontal acceleration less than 1% of the vertical one). The sinusoidal gravity modulation $g_{eff}(t) = a_{ex}\cos(2\pi f_{ex}t)$ is measured by a piezoelectric accelerometer (Acc) and a charge amplifier, where a_{ex} is proportional to the applied tension with a 1.0 Vs^2/m sensitivity and f_{ex} is the excitation frequency. A biaxial tilt sensor

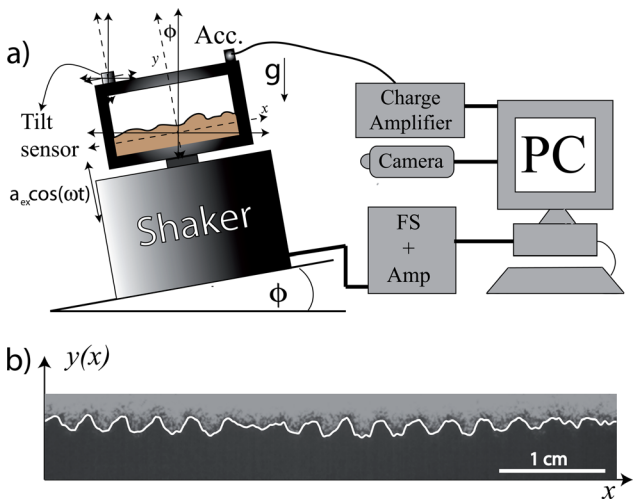

FIG. 4. Granular drifting patterns. (a) Schematic representation of the experimental setup. (b) Typical snapshot of the granular pattern. The continuous white line corresponds to the numerically calculated granular interface.

driven by a 12 V power supply is positioned solidary on top of the cell in order to measure the inclination of the cell with respect to the axis of gravity in the $x-y$ plane with a sensitivity of 100 mV/°. This inclination is represented by the angle ϕ (cf. Fig. 4). In this experimental configuration, ϕ is monitored by measuring the x-axis voltage difference. The variations of the off-plane inclination angle on the x-axis are also monitored to ensure that only in-plane movements of the cell are allowed. The control parameters are the forcing frequency f_{ex}, the acceleration amplitude a_{ex}, and the in-plane inclination angle ϕ. Images were acquired at 20 fps over 100 s using a CCD camera over a 120×840 px window (6.5×10^{-3} cm/px sensitivity in the horizontal direction and 6.3×10^{-3} cm/px in the vertical direction). Using a simple tracking scheme,[21] the granular pattern interface $y(x,t)$ is computed (as shown in Fig. 4(b)), where x corresponds to the spatial coordinate along the x-axis and t to the temporal one. Using this data, the local envelope, phase gradient, and velocity are obtained. In this work, we focused solely on the characterization of the spatiotemporal dynamics of the subharmonic standing waves formed on top of the quasi-one-dimensional fluidized shallow granular bed appearing through a supercritical parametric instability[22,23] as a certain acceleration threshold of the container is surpassed. To do this, the excitation parameters are fixed at $f_{ex} = 40$ Hz, and $a_{ex} = 58\ \text{m/s}^2$, which is ~20% larger than the critical acceleration for subharmonic patterns at f_{ex}.

Dislocation chains appear locally in the spatiotemporal diagram of the pattern evolution,[24] as it is depicted in Fig. 5. These dislocations, appearing isolated or in groups, can be clearly pinpointed as we compute the phase gradient of pattern $\partial_x\varphi$ (cf. Fig. 5(b)). In our experimental setup, due to the horizontal inclination angle of the cell[9] and the intrinsic heaping of the system arising from air-grain interactions,[25] inhomogeneous drift force appears (cf. Fig. 5), which can be measured by the local time-averaged phase speed of the pattern (cf. Fig. 5(c)). The local averaged phase speed is obtained by two independent methods: the Hilbert transform

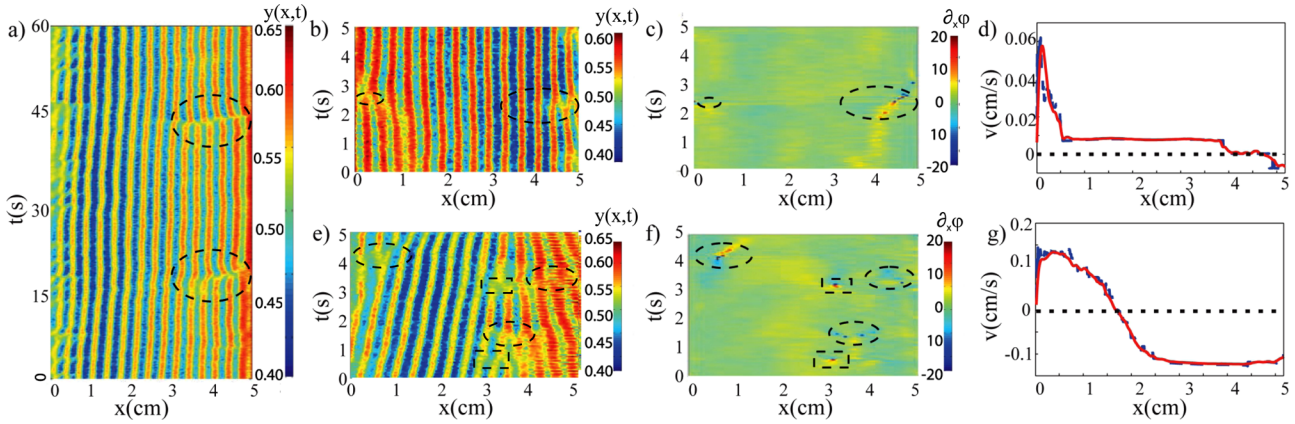

FIG. 5. Experimental dislocation chains. (a) Drifting pattern with long dislocation chains (dashed ovals) for $\phi = 0.07°$. (b) Drifting pattern for $\phi = 0.02°$. (c) Local phase gradient. Dashed squares represent isolated defects and dashed circles dislocation chains. (d) Local velocity averaged over the entire image sequence. The continuous line corresponds to the velocity computed using a rigid solid approximation (see Ref. 27) and the dashed line using a Hilbert transform. (e) Drifting pattern for $\phi = 0.15°$. (f) Local phase gradient. Dashed squares represent isolated defects and dashed circles dislocation chains. (g) Local velocity averaged over the entire image sequence. The continuous line corresponds to the velocity computed using a rigid solid approximation (see Ref. 27) and the dashed line using a Hilbert transform.

algorithm[26] and the rigid solid method.[27] For very small inclination angle ϕ, the dominant mechanism for the generation of drift forces are inhomogeneities created by the air-grain interactions such as heaping (speed jumps, see Fig. 5(d)). For $\phi > 0.5°$, contrarily, the horizontal inclination leads the dynamics (counter flows, see Fig. 5(g)). For intermediate angles, both mechanisms contribute to generate inhomogeneities in the speed profile. It must be stressed that without inhomogeneous drift force, no defects are observed in the stationary pattern. Figure 5 shows, respectively, the stroboscopic spatiotemporal diagram of $y(x,t)$ acquired at $f_{ex}/2$, $\phi = 0.02°$ (top) and $\phi = 0.15°$ (bottom). We observe that for the counter-propagative flow (cf. bottom panel Fig. 5) or speed jumps (cf. top panel Fig. 5), the spatiotemporal diagrams of fluidized shallow granular bed show the emergence of dislocations. These dislocations, which are singularities in the local phase of the pattern, appear in the region where the speed of the pattern presents substantial spatial variations (see Fig. 5(g)). Hence, in these regions, the drifting pattern manifests a phase instability that leads to the emergence of phase singularities. As we have mentioned, analogous spatiotemporal diagrams have been reported in particle-laden flows inside a partially fluid filled, horizontal, rotating cylinder,[13] a free electron laser,[14] and a one-dimensional transverse Kerr-type slice subjected to optical feedback.[15] Therefore, spatiotemporal dislocation chains are a robust phenomenon displayed by pattern forming systems in the presence of inhomogeneous forcing.

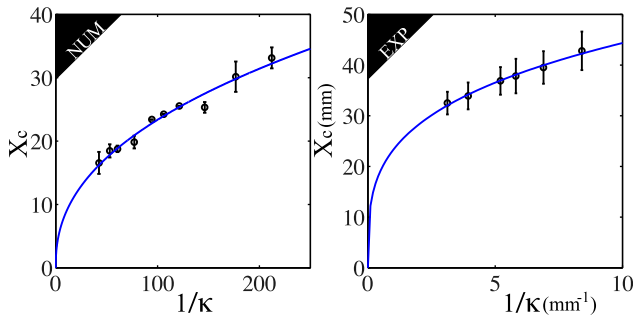

FIG. 6. Plot of X_c vs κ^{-1} obtained by numerical simulations (left) and direct experimental measurements (right). Continuous lines are numerical fits.

To complete our analysis, we perform a numerical and experimental verification of the theoretical prediction for X_c, Formula (9). As seen in Fig. 6 (left panel), numerical simulations of the amplitude Eq. (3) exhibit a power law of the form $X_c = a(1/\kappa)^b$ with $a = 3.25$ y $b = 0.43 \pm 0.05$ close to the expected critical exponent $b = 0.5$ of expression (9). The experimental verification in drifting granular patterns shows a deviation of the predicted behavior, exhibiting a power law $X_c = a(1/\kappa)^b$ with $a = 23.29$ y $b = 0.28 \pm 0.1$ [see Fig. 6 (right panel)]. Such deviation can be due to the fact that the inhomogeneous drift does not follow a linear profile in space [Figs. 5(d) and 5(g)]. Notwithstanding, we can approximate in some limit this profile to a linear ramp close to the confluence region $X_0 = 0$. An additional effect that can modify this scale-invariant behavior is defect interaction that is not included in the above approach.

V. CONCLUSION

We have shown that the complex spatiotemporal dynamics exhibited by inhomogeneous drifting patterns can be figured out as a perpetual phase singularity production resulting from phase instabilities (coming from a local Eckhaus instability) and pattern propagation induced by an inhomogeneous drift force. Thus, inhomogeneities in spatial coupling are the origin of this phenomenon. Hence, this rich and complex spatiotemporal dynamics can be understood as a combination of simple phenomena. The experimental findings of the spatiotemporal dynamics of dislocation chains are in quite good agreement with our theoretical general description valid for a broad class of physical systems. The study of the effect of fluctuations (noise) on the spatiotemporal dynamics of phase singularities and their interactions is a work in progress.

ACKNOWLEDGMENTS

The authors acknowledge financial support by the ANR-CONICYT 39, "*Colors*". M.G.C., M.A.G-N., C.F., and V.O. thank for the financial support of FONDECYT projects 1120320, 3110024, 1130354, and 3130382, respectively.

[1]G. Nicolis and I. Prigogine, *Self-Organization in Non Equilibrium Systems* (Wiley, New York, 1977).
[2]M. C. Cross and P. C. Hohenberg, Rev. Mod. Phys. **65**, 851, (1993).
[3]L. M. Pismen, *Patterns and Interfaces in Dissipative Dynamics* (Springer Series in Synergetics, Berlin, 2006).
[4]M. I. Rabinovich, A. B. Ezersky, and P. D. Weidman, *The dynamics of Patterns* (World Scientific, Singapore, 2000).
[5]M. Cross and H. Greenside, *Pattern Formation and Dynamics in Nonequilibrium Systems* (Cambridge University Press, New York, 2009).
[6]P. Coullet and G. Iooss, Phys. Rev. Lett. **64**, 866 (1990).
[7]C. Godreche and P. Manneville, *Hydrodynamics and Nonlinear Instabilities* (University Press, Cambridge, 1998).
[8]T. Epstein and R. D. Deegan, Phys. Rev. E **81**, 066310 (2010).
[9]J. Garay, I. Ortega, M. G. Clerc, and C. Falcón, Phys. Rev. E **85**, 035201(R) (2012).
[10]D. R. Ohlsen, S. Y. Yamamoto, C. M. Surko, and P. Kolodner, Phys. Rev. Lett. **65**, 1431 (1990); J. Stat. Phys. **64**, 903 (1991); H. U. Voss, P. Kolodner, M. Abel, and J. Kurths, Phys. Rev. Lett. **83**, 3422 (1999).
[11]M. G. Clerc, C. Fernandez-Oto, M. A. Garcia-Ñustes, and E. Louvergneaux, Phys. Rev. Lett. **109**, 104101 (2012).
[12]R. E. Goldstein, G. H. Gunaratne, L. Gil, and P. Coullet, Phys. Rev. A **43**, 6700 (1991).
[13]E. Guyez and P. J. Thomas, Phys. Rev. Lett. **100**, 074501 (2008); G. Seiden and P. Thomas, Rev. Mod. Phys. **83**, 1323 (2011).
[14]S. Bielawski, C. Szwaj, C. Bruni, D. Garzella, G. L. Orlandi, and M. E. Couprie, Phys. Rev. Lett. **95**, 034801 (2005).
[15]E. Louvergneaux, Phys. Rev. Lett. **87**, 244501 (2001).
[16]H. Riecke and H. G. Paap, Phys. Rev. Lett. **59**, 2570 (1987).
[17]C. Normand, Y. Pomeau, and M. G. Velarde, Rev. Mod. Phys. **49**, 581(1977).
[18]S. A. Akhmanov, M. A. Vorontsov, and V. Yu. Ivanov, JETP Lett. **47**, 707 (1988).
[19]G. DAlessandro and W. Firth, Phys. Rev. A **46**, 537 (1992).
[20]E. Hairer, S. P. Norsett, and G. Wanner, *Springer Series in Computational Mathematics* (Springer, Berlin, 1993).
[21]I. Ortega, M. G. Clerc, C. Falcon, and N. Mujica, Phys. Rev. E **81**, 046208 (2010).
[22]M. Faraday, Philos. Trans. R. Soc. London **121**, 299 (1831).
[23]I. Aronson and L. Tsimring, *Granular Patterns* (Oxford University Press, 2009).
[24]See supplementary material at http://dx.doi.org/10.1063/1.4883650 for a movie that shows spatiotemporal dislocation chains in the system.
[25]H. K. Pak, E. Van Doorn, and R. P. Behringer, Phys. Rev. Lett. **74**, 4643 (1995).
[26]J. Claerbout, *Fundamentals of Geophysical Data Processing* (McGraw-Hill, 1976).
[27]The rigid solid method is based upon an optimization principle for speed and shape of the local profile using a Gaussian-weighted spatial average function. An explanation of the method can be found in http://www.tesis.uchile.cl/handle/2250/115494.